CRYSTAL GROWTH & DESIGN

ACS AuthorChoice

Communication

pubs.acs.org/crystal

Role of $CaCO_3^\circ$ Neutral Pair in Calcium Carbonate Crystallization

Damiano Genovese,[‡] Marco Montalti,[‡] Fermín Otálora,[†] Jaime Gómez-Morales,[†] María Sancho-Tomás,[†] Giuseppe Falini,[‡] and Juan Manuel García-Ruiz*[,†]

[†]Laboratorio de Estudios Cristalográficos, Instituto Andaluz de Ciencias de la Tierra (CSIC-UGR), Avda. Las Palmeras, no 4, 18100 Armilla (Granada), Spain

[‡]Dipartimento di Chimica "G. Ciamician", Alma Mater Studiorum Università di Bologna, via Selmi 2, I-40126 Bologna, Italy

Supporting Information

ABSTRACT: The molecular structure of the units that get incorporated into the nuclei of the crystalline phase and sustain their growth is a fundamental issue in the pathway from a supersaturated solution to the formation of crystals. Using a fluorescent dye we have recorded the variation of the pH value in time along a gel where $CaCl_2$ and $NaHCO_3$ counter-diffuse to crystallize $CaCO_3$. The same pH−space−time distribution maps were also computationally obtained using a chemical speciation code (phreeqc). Using data arising from this model we investigated the space-time evolution of the activity of the single species (ions and ion pairs) involved in the crystallization process. Our combined results suggest that, whatever the pathway from solution to crystals, the neutral pair $CaCO_3^\circ$ is a key species in the $CaCO_3$ precipitation system.

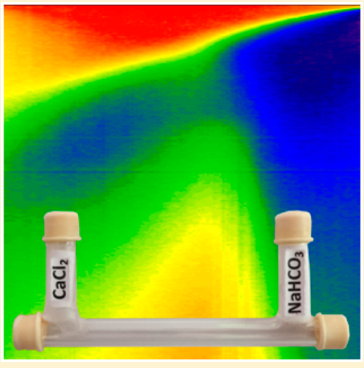

The correct understanding of the nature (ionic or molecular) and chemical composition of the growth units building the crystals is important for a wide variety of crystallization processes ranging from biological mineralization to materials synthesis. Obtaining this knowledge from crystallization experiments is rather difficult since it is mandatory to find experimental evidence of these primary species. In this work we face such a challenge using the crystallization of calcium carbonate ($CaCO_3$) as a model system. This case has been chosen because (i) the reactions between calcium ions and inorganic carbon may form many solution species that could either be the crystal building units or control their concentration; (ii) thermodynamic and kinetic data on the precipitation of $CaCO_3$ is widely available; (iii) $CaCO_3$ has important implications in industrial, technological, environmental, and biological processes and its nucleation and growth mechanisms are nowadays a matter of intense debate;[1−10] (iv) the precipitation of $CaCO_3$ is a pH controlled process and can be monitored by pH probes.

This dependence on pH is the first key point for our work, because it opens a window to the otherwise elusive problem of identifying the solution species. The evolution of pH over time has certainly been recorded many times in $CaCO_3$ precipitation studies. In commonly used precipitation methods, such as titration and direct mixing of a calcium ion solution with either a carbonated solution or CO_2 gas, only a time series of volume-averaged pH values can be recorded. The information provided by these volume-averaged measurements does not inform about the space distribution of soluble species playing a role during the crystallization process.

Thus, the second key point of our work is using the counterdiffusion (CD) method instead of direct mixing. In CD experiments the distribution of aqueous species is unfolded along a one-dimensional space.[11−13] This allows the recording of thousands of pH values in different points and at different times to build a spatiotemporal map of the pH distribution. In CD crystallization of calcium carbonate two solutions, one containing hydrogen carbonate ions and the other calcium ions are allowed to counterdiffuse through a gel matrix or high-viscosity fluid.[14−16] The diffusion of the different chemical species leads to the development of species concentration gradients that evolve over time. The CD method has been traditionally used to optimize the size and quality of crystals for X-ray diffraction experiments (either from small molecules or macromolecules),[17,18] but their capabilities for space−time unfolding of experimentally measured values has seldom been explored.

pH is one of these unfolded values, and the one we use in our work. The last key ingredient of our study is the development of an experimental method to measure in situ the pH distribution in a crystallization experiment by using a pH sensitive fluorescent dye embedded in the gel. Using this pH imaging capability to track the evolution of a $CaCO_3$ crystallization experiment by CD, we have produced space- and time-resolved maps of pH. These maps are made of thousands of measurements so they can be confidently compared with the output of transport/speciation simulations

Received: February 19, 2016
Revised: May 20, 2016
Published: July 8, 2016

DOI: 10.1021/acs.cgd.6b00276
Cryst. Growth Des. 2016, 16, 4173−4177

to derive conclusions and support hypotheses on the distribution of species in solution. Using this combined method we have derived the activity of all inorganic aqueous species revealing the key role of the neutral pair $CaCO_3^\circ$ in the crystallization of $CaCO_3$.

CD experiments have been carried out within U-tubes (Figure 1a). The two vertical branches were filled respectively

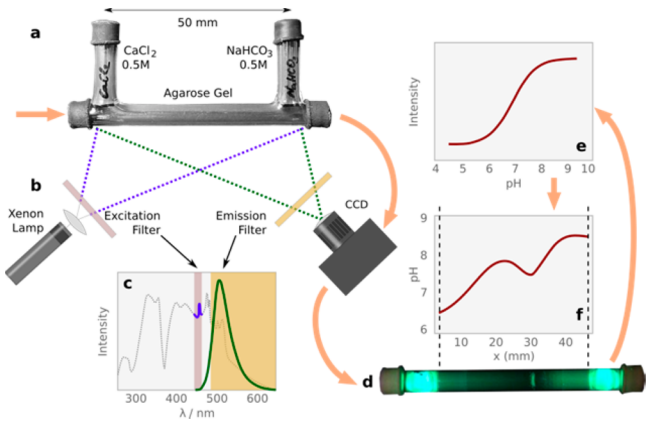

Figure 1. Experimental procedure for pH measurements: (a) U-tube setup used for $CaCO_3$ crystallization by CD method. (b) Optical setup: a narrow bandpass filter (pink) is used to select a wavelength of 450 nm (blue/purple in the figure) from the xenon lamp illumination. This radiation excites green fluorescence (green in the figure) in the pH sensitive ink. This radiation is selectively collected through a bandpass filter (brown in the figure) and imaged on a CCD. (c) Plot showing the wavelength filtering previously described; absorbance and emission curves are included for both the protonated and deprotonated ink along with their spectral position with respect to filters. (d) Raw fluorescence image as collected by the CCD. These images are quantitatively analyzed using a calibration curve (e) to produce the final pH profile (f). Plots (c) and (e) are available in the Supporting Information (SI3 and SI4).

with 0.5 M solutions of the two reagents, sodium hydrogen carbonate ($NaHCO_3$) (right arm) and calcium chloride ($CaCl_2 \cdot 2H_2O$) (left arm). The horizontal segment of the U-tube was filled with 3% (w/w) agarose gel containing the pH-fluorescent dye (8-hydroxypyrene-1,3,6-trisulfonic acid trisodium salt). The time evolution of the pH has been obtained from time-lapse series pictures following the procedure shown in Figure 1. Speciation, mass transport, and precipitation have been simulated using the Phreeqc code (v 3.1.4).[19−22] Species activities have been calculated using ion association with thermodynamic data from the Phreeqc.dat database. Mass transport was simulated using the multicomponent diffusion algorithm in Phreeqc. In counterdiffusion experiments, the ionic activity product increases slowly. In these conditions the first polymorph produced is always calcite, as confirmed in a previously reported experiment.[16] Therefore, only this crystalline phase was considered in the model. Agarose gel is not included in the solution chemistry, because although it is physically embedded into the crystals during their growth, it has no influence on chemical speciation. All details of the experiment (SI1) and the Phreeqc input file used in the simulation (SI2) are available in the Supporting Information.

Figure 2 (left) displays a map showing the variation of pH in time (vertical axis) and space (horizontal axis) recorded during the crystallization experiment. The initial pH of the horizontal agarose-filled segment is 6.5 (red-orange in color scale). Once

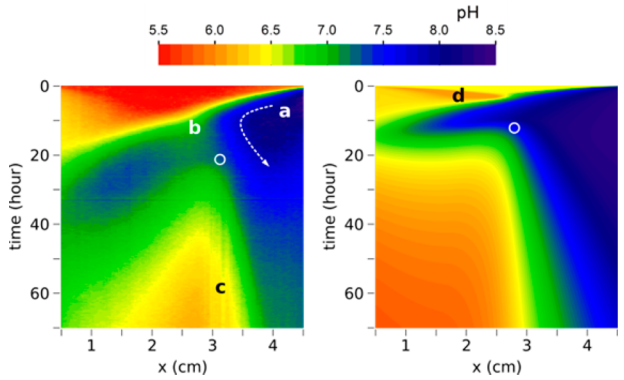

Figure 2. Experimental (left) and calculated (right) maps of pH−space−time. The color scale for pH is shown on top of the left map. The circle marks the position and the time where first nucleation occurs. Dashed line with white arrows marks the evolution in time of the alkaline front at pH ∼ 8. The horizontal dotted lines indicate the time for which the species activity is plotted in Figure 3.

diffusion of ions starts, the pH of the right part of the agarose gel increases upon arrival of HCO_3^-/CO_3^{2-} ions (color shifts quickly from red to dark blue, see label "a" in figure). At the left part of the gel tube the diffusion of Ca^{2+} in the opposite direction keeps the pH acidic, but progressively, the arriving HCO_3^-/CO_3^{2-} ions start to increase the local pH. On the right part, the increment of pH creates an alkaline front that penetrates across the tube following a classical diffusion profile. Close to the center of the tube, a decrease of pH produced by chemical reactions between the incoming ions is observed (label "b"). Dashed lines with white arrows mark the evolution in time of the alkaline front at pH ∼8.

The location of the first forming crystals was observed by optical microscopy time-lapse images, but also from the pH versus space/time map, because as soon as the crystals reached a critical size of a few hundred nanometers they started to scatter light that, when recorded at the detector, shows as an apparent local decrease of pH in the map (label "c"). The circle in Figure 2 (left) marks the position and the time where the first crystals are observed.

This complex experimental pH distribution in space and time is notably well reproduced by the simulation output (Figure 2, right). Apart from some minor differences like the pH minimum moving from left to right (label "d") that is less prominent but present in the experiment or the apparent pH decrease at positions where crystals are growing (label "c"), the only difference between the experiment and the model is the time (vertical) scale. The multicomponent diffusion algorithm[21] implemented in Phreeqc was used in our model because the diffusion coefficients (unknown for most solution species) are computed ab initio and because ion transport is corrected by ensuring electrical neutrality over the solution volume. This ab initio computation of diffusion coefficients is based on tracer diffusion that is too fast for real solution diffusing through a gel. This overestimation of the diffusion coefficients produces a compression of the time dimension in the model output. The model assumes no nucleation barrier: calcium carbonate starts to precipitate as soon as it is supersaturated. This strategy was chosen to avoid the use of free parameters of kinetic nature in the model, and also contributes to the earlier nucleation events in the model. The fact that this complex pH landscape is notably reproduced by an speciation simulation with simple mass transport and chemical equilibrium equations suggests

DOI: 10.1021/acs.cgd.6b00276
Cryst. Growth Des. 2016, 16, 4173−4177

that the pH evolution and the onset of calcium carbonate precipitation is controlled by the distribution of species in solution. In order to explain these maps and to understand the precipitation behavior of $CaCO_3$, one needs to know the spatial-temporal distribution of all solution species and their mutual interactions. The output of the simulation records each second at 100 points along the tube the concentration and activity of the following species: H^+, OH^-, Cl^-, Na^+, Ca^{2+}, CO_2, HCO_3^-, CO_3^{2-}, $CaHCO_3^+$, $CaCO_3^\circ$, $CaOH^+$, $NaCO_3^-$, $NaHCO_3$, and NaOH. Maps of these species are available in the Supporting Information (SI5). Among them, $CaCO_3^\circ$ and $CaHCO_3^+$ (along with pH) were found the most relevant for the problem at hand. $Ca(HCO_3)_2$, that forms at lower pHs (<6),[20] may form at concentrations much smaller than the major species and play no role in the overall speciation process. More complex species like polymers or clusters of the relevant pairs have not been considered in the calculations because their formation is not described by equilibrium chemical reactions, which is what the code computes.

Figure 3 shows profiles of these species at times well before nucleation (1 h), right before nucleation (8 h), and after nucleation (14 h). These times are marked as white horizontal dotted lines in Figure 2 (right). The full time evolution is illustrated as a movie (SI6) in the Supporting Information.

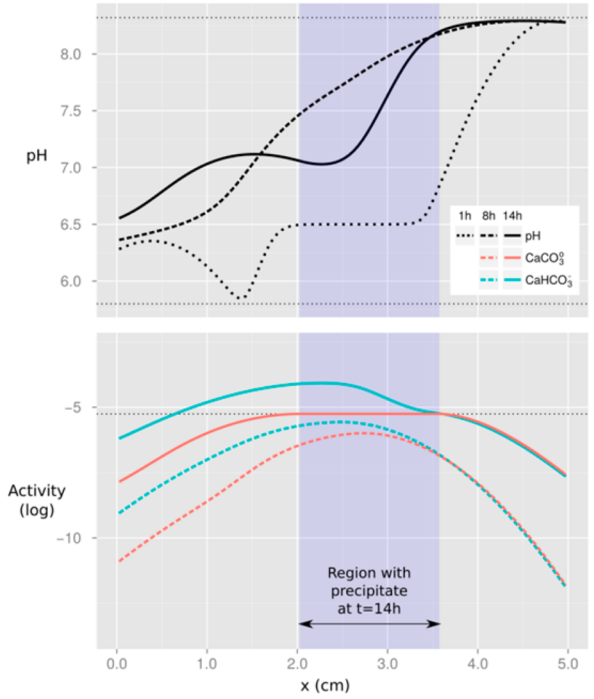

Figure 3. Evolution in time of pH (black lines) and activities of $CaHCO_3^+$ (blue lines) and $CaCO_3^\circ$ (orange lines) along the gel tube. For the sake of clarity only plots after 1 h (dotted lines), 8 h (dashed lines), and 14 h (continuous lines) are shown. The full time evolution is illustrated as a movie (SI6) in the Supporting Information. The thin horizontal dotted lines in the pH plot (top) represent the simulation input pH values in both reservoirs. The thin horizontal dotted line intercepting the *log activity* axis (bottom plot) at −5.26 represent the $CaCO_3^\circ$ critical activity value for precipitation.

One hour after starting the experiment, the pH profile is dominated by the presence of Ca^{2+} and HCO_3^- because the activity of each of them is negligible in all places where the activity of the other is high. The activity of CO_3^{2-} at that time is very low compared to that of HCO_3^-. The minimum of pH close to the cationic reservoir (left in the plot) is due to the hydrolysis of Ca^{2+}, which drives the pH value close to 5.8 (lower dotted horizontal line) according to the equilibrium[23]

$$Ca^{2+} + H_2O \leftrightarrow Ca(OH)^+ + H \qquad \log K_h = -12.8 \tag{1}$$

Close to the anionic reservoir, the diffusion of HCO_3^- raises the initial pH of the gel (6.5) up to 8.3 (the upper dotted line).

As the counterdiffusion process continues diffusing Ca^{2+} to the right and CO_3^{2-}/HCO_3^- to the left, new species in solution start forming (Figure 3, bottom) according to equilibria[24]

$$Ca^{2+} + CO_3^{2-} \leftrightarrow CaCO_3^\circ \qquad \log K_{CaCO_3^\circ} = 3.22 \tag{2}$$

$$Ca^{2+} + HCO_3^- \leftrightarrow CaHCO_3^+ \qquad \log K_{CaHCO_3^+} = 1.11 \tag{3}$$

As shown in the plot (bottom of Figure 3) as well as in movie SI6, the activities of both pairs increase continuously. The first solid $CaCO_3$ is formed when the activity of $CaCO_3^\circ$ reaches a critical value (thin horizontal dotted line in the bottom plot). After this event, the $CaCO_3^\circ$ activity, in the region where crystals are nucleating and growing (marked by the vertical blue rectangle), remains constant at the critical value level (the flat top of the orange curve), indicating that this species is being produced and consumed at the same rate. The maximum activity of $CaHCO_3^+$ is to the left of the crystallization region and keeps increasing after solid $CaCO_3$ is formed instead of remaining constant (Figure 3). In the same region, after the first precipitation, Ca^{2+} and CO_3^{2-} activities diverge over time while the ionic product is kept constant, as expected (Figure 4). The evolution of the activities of both pairs in a scenario rich in Ca^{2+} and HCO_3^- ions indicates that neutral $CaCO_3^\circ$ is consumed in the process of calcium carbonate crystallization while charged $CaHCO_3^+$ acts as an alternative reservoir contributing ions to form $CaCO_3^\circ$ in addition to the Ca^{2+} and CO_3^{2-} supplied by counterdiffusion. Note that the overall equilibrium 5, that delivers neutral pairs on demand, is a combination of equilibria 2, 3, and 4. The released protons yield the pH minimum that can be observed at 14 h (Figure 3, solid black line) at the crystallization region. This release of protons also keeps increasing the concentration of $CaHCO_3^+$ according to[24]

$$HCO_3^- \leftrightarrow CO_3^{2-} + H^+ \qquad \log K_2 = -10.33 \tag{4}$$

$$CaHCO_3^+ \leftrightarrow CaCO_3^\circ + H^+ \qquad \log K = -8.22 \tag{5}$$

The relevance of ion pairs in the dissolution and precipitation processes of $CaCO_3$ was already theoretically suggested. Plummer and Busenberg[24] showed that the experimental values of solubility equilibrium constants of $CaCO_3$ polymorphs are consistent with an aqueous model including $CaCO_3^\circ$ and $CaHCO_3^+$. Gómez-Morales et al.[25] found that, by maintaining the ionic activity product constant, the maximum nucleation rate (minimum induction time) occurred in solutions with initial stoichiometric Ca^{2+}/CO_3^{2-} concentrations, whereas maximum growth rate occurred in the experiments with excess of Ca^{2+}; the activities of $CaCO_3^\circ$ in solution and at the crystal surface respectively were found to be

DOI: 10.1021/acs.cgd.6b00276
Cryst. Growth Des. 2016, 16, 4173−4177

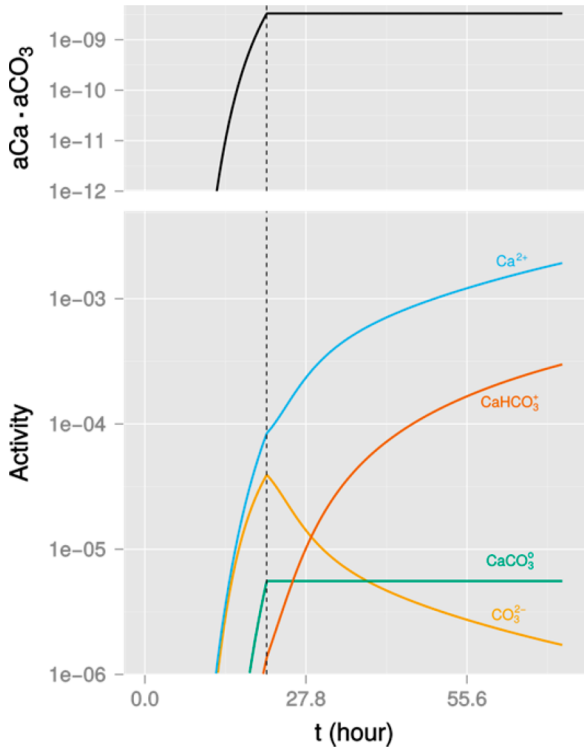

Figure 4. Time evolution of activity for the ions Ca^{2+}, CO_3^{2-} and the pairs $CaHCO_3^+$, $CaCO_3^\circ$ (bottom). The ionic activity product $a(Ca^{2+})\ a(CO_3^{2-})$ is shown in the top panel.

maximized in these conditions, so they proposed that the activities of $CaCO_3^\circ$ in solution and on the crystal surface are rate limiting for nucleation and growth, respectively. Ruiz-Agudo et al.[26] also suggested that the $CaCO_3^\circ$ should play an important role in crystal growth of calcium carbonate on the basis of its smaller degree of hydration that would facilitate the incorporation in the structure by making it faster. Additionally, it has been experimentally shown that the Ca^{2+}/CO_3^{2-} molar ratio in solution, affecting the concentrations of $CaCO_3^\circ$ and $CaHCO_3^+$, strongly influences the growth rate of calcite.[27,28] Our results indicate that among the two pairs only $CaCO_3^\circ$ is consumed in equilibrium during the precipitation process. Whether $CaCO_3^\circ$ or a larger neutral cluster formed by aggregation of these discrete species is the relevant growth unit cannot be derived from our findings, since clustering is not considered in the calculations.

Our model, based on equilibrium calculations, logically implies that the ionic activity product of Ca^{2+} and CO_3^{2-} must be constant when the activity of the neutral pair is constant, and this is what we observed (Figure 4). Therefore, we cannot conclusively determine whether the calcium/carbonate ions or the neutral pair are the units whose aggregations feeds calcite nucleation and growth, but both the previous reports on this subject[25,29] and the evolution of the Ca^{2+} and CO_3^{2-} concentration after nucleation do support the hypothesis of $CaCO_3^\circ$ being the most likely candidate. The activities of Ca^{2+} and CO_3^{2-} diverge after the first precipitate forms. At the first nucleation, their activities are very similar and both increase with time, but after this event, the activity of Ca^{2+} keeps increasing while that of CO_3^{2-} starts to decrease quickly. The ratio Ca^{2+}/CO_3^{2} changes from around 1 a few hours before nucleation to 100 a few hours after nucleation and more than 1000 1 day after.

In this strongly nonstoichiometric situation, an expression for supersaturation as a function of the activity of the $CaCO_3^\circ$ instead of the lattice ions could be more realistic to define the rate equations in calcium carbonate precipitation.

From a chemical point of view, calcium binding to HCO_3^- through monodentate interaction or to CO_3^{2} through a bidentate interaction modifies the coordination of the hydrated calcium. The strongest bidentate interaction of carbonate explains why this anion, rather than bicarbonate, is the one entering the elemental building brick even though bicarbonate is the prevailing anion in solution.[30]

Besides the interest of the plausible role of $CaCO_3^\circ$ as the calcite growth unit, these results can also shed light on the onset of $CaCO_3$ crystallization process (nucleation). In the classical view, the nucleation is a stochastic process in which fluctuations induce the formation of clusters that evolve by accretion of discrete units. In the case of calcium carbonate, our results suggest that instead of calcium and carbonate ions, these units can be $CaCO_3^\circ$ following the reaction

$$CaCO_3^\circ \leftrightarrow CaCO_3(s) \tag{6}$$

Gebauer et al.,[3] by using titration and ultracentrifugation techniques, demonstrated the formation of $(CaCO_3)_x$ pre-nucleation clusters. According to their model the nucleation follows a nonclassical pathway and $CaCO_3$ forms by aggregation of these clusters. Our results suggest the formation of these neutral clusters could take place by aggregation of $CaCO_3^\circ$ as an intermediate step toward the formation of solid $CaCO_3$.

$$CaCO_3^\circ \leftrightarrow (CaCO_3)_x \leftrightarrow CaCO_3(s)$$
$$\text{with } x = 1, 2, 3, \ldots, n \tag{7}$$

Wallace et al.,[5] by using molecular dynamics simulations, reported that previously formed clusters adopt chain, ring, and branched structures. They predict the formation of nanoscale droplets in concentrated solutions by liquid−liquid phase separation.[4] These droplets coalesce and solidify to form the solid phase, amorphous calcium carbonate.

Neither clustering processes nor liquid−liquid separation are considered in our calculations. However, the identification of $CaCO_3^\circ$ as a key species involved in $CaCO_3$ precipitation may reconcile both views, the nonclassical where large neutral clusters $(CaCO_3)_x$ form and the classical where both solid nuclei and $CaCO_3^\circ$ in solution do form from the same ions.

The fact that $(CaCO_3)_x$ or $CaCO_3^\circ$ can be the key species in $CaCO_3$ crystallization has important implications in the understanding of precipitation phenomena. According to eq 7, and considering $x = 1$, the supersaturation β of the solution with respect to the most stable polymorph, calcite, should be expressed as

$$\beta = \frac{(a_{CaCO_3^\circ})_{actual}}{(a_{CaCO_3^\circ})_{equilibrium}} = \frac{(a_{CaCO_3^\circ})_{actual}}{K_{CaCO_3^\circ} K_{sp}} \tag{8}$$

with K_{sp} (calcite) = $10^{-8.48}$,[24] instead of the usual expression in terms of the ionic activity product (IAP) and solubility product (K_{sp}). Letting $\beta = 1$ in eq 7, the equilibrium $CaCO_3^\circ$ activity can be computed to be 10^{-5}.[26] This is the critical activity value that should be overtaken to produce solid $CaCO_3$ (horizontal dotted line in Figure 3). In macroscopic equilibrium experiments both approaches are obviously equivalent, but the finding of $(CaCO_3)_x$ as a relevant species for $CaCO_3$

DOI: 10.1021/acs.cgd.6b00276
Cryst. Growth Des. 2016, 16, 4173−4177

crystallization is expected to have a deeper impact in situations where the interactions at the molecular scale are relevant as in molecular dynamics studies; the distribution of solution species is unsteady, as in counterdiffusion experiments, where the calcium to carbonate ratio changes over time and along space; and the ionic strength and type of electrolyte added change or additives that can modify the speciation equilibria are present.

In these situations a critical reexamination considering the neutral cluster $(CaCO_3)_x$ species as the primary building unit for $CaCO_3$ crystallization can bring new insights into unexpected or unexplained precipitation behaviors and open new possibilities for controlling the nucleation and growth of calcium carbonate.

■ ASSOCIATED CONTENT

Supporting Information

The Supporting Information is available free of charge on the ACS Publications website at DOI: 10.1021/acs.cgd.6b00276.

Experimental and simulation methods; wavelength spectra and filtering; fluorescence intensity vs solution pH calibration; space/time maps for additional solution species; movie of time evolution of pH, $CaHCO_3^+$, $CaCO_3^\circ$ (PDF)

■ AUTHOR INFORMATION

Corresponding Author

*E-mail: juanma.garciaruiz@gmail.com.

Author Contributions

The manuscript was written through contributions of all authors.

Notes

The authors declare no competing financial interest.

■ ACKNOWLEDGMENTS

This work was performed within the framework of the projects: European Research Council (European Union's Seventh Framework Programme (FP7/2007-2013) grant agreement no 340863, and Spanish MINECO grants MAT2014-60533-R and CGL2010-16882 cofounded with FEDER. M.S.T. acknowledges CSIC for her JAE-Pre contrat cofunded by the European Social Fund. All coauthors thank James J. De Yoreo and Helmut Cölfen for the fruitful discussion of the results of this work.

■ ABBREVIATIONS

CD, counterdiffusion; CCD, charged coupled device; equil, equilibrium (in eq 7)

■ REFERENCES

(1) Gebauer, D.; Coelfen, H. *Nano Today* **2011**, *6*, 564−584.
(2) Navrotsky, A. *Proc. Natl. Acad. Sci. U. S. A.* **2004**, *101*, 12096−12101.
(3) Gebauer, D.; Voelkel, A.; Coelfen, H. *Science* **2008**, *322*, 1819−1822.
(4) Gower, L. B. *Chem. Rev.* **2008**, *108*, 4551−4627.
(5) Wallace, A. F.; Hedges, L. O.; Fernandez-Martinez, A.; Raiteri, P.; Gale, J. D.; Waychunas, G. A.; Whitelam, S.; Banfield, J. F.; De Yoreo, J. J. *Science* **2013**, *341*, 885−889.
(6) Gebauer, D.; Kellermeier, M.; Gale, J. D.; Bergström, L.; Cölfen, H. *Chem. Soc. Rev.* **2014**, *43*, 2348−2371.
(7) Tribello, G. A.; Bruneval, F.; Liew, C. C.; Parrinello, M. *J. Phys. Chem. B* **2009**, *113*, 11680−11687.
(8) Raiteri, P.; Gale, J. D. *J. Am. Chem. Soc.* **2010**, *132*, 17623−17634.
(9) Demichelis, R.; Raiteri, P.; Gale, J. D.; Quigley, D.; Gebauer, D. *Nat. Commun.* **2011**, *2*, 590.
(10) General discussion. *Faraday Discuss.* **2012**, *159*, 387−420.10.1039/c2fd90027k
(11) Otálora, F.; García-Ruiz, J. M. *J. Cryst. Growth* **1996**, *169*, 361−367.
(12) Otálora, F.; García-Ruiz, J. M. *J. Cryst. Growth* **1997**, *182*, 141−154.
(13) García-Ruiz, J. M.; Otálora, F.; Novella, M. L.; Gavira, J. A.; Sauter, C.; Vidal, O. *J. Cryst. Growth* **2001**, *232*, 149−155.
(14) Henisch, H. K.; García-Ruiz, J. M. *J. Cryst. Growth* **1986**, *75*, 203.
(15) Prieto, M.; Fernández-Díaz, L.; López-Andrés, S. *J. Cryst. Growth* **1991**, *108*, 770−778.
(16) Sancho-Tomás, M.; Fermani, S.; Durán-Olivencia, M. A.; Otálora, F.; Gómez-Morales, J.; Falini, G.; García-Ruiz, J. M. *Cryst. Growth Des.* **2013**, *13*, 3884−3891.
(17) García-Ruiz, J. M. *Methods Enzymol.* **2003**, *368*, 130−154.
(18) Otálora, F.; Gavira, J. A.; Ng, J. D.; García-Ruiz, J. M. *Prog. Biophys. Mol. Biol.* **2009**, *101*, 26−37.
(19) Parkhurst, D. L.; Appelo, C. A. J. in *U.S. Geological Survey Techniques and Methods* 2013; book 6, chap. A43; available only at http://pubs.usgs.gov/tm/06/a43/.
(20) Bashkin, V. N. *Environmental Chemistry: Asian Lessons*; Kluwer Academy Publishers: Dordrecht, The Netherlands, 2003; p 221.
(21) Vinograd, J. R.; McBain, J. W. *J. Am. Chem. Soc.* **1941**, *63*, 2008−2015.
(22) Appelo, C. A. J.; Wersin, P. *Environ. Sci. Technol.* **2007**, *41*, 5002−5007.
(23) Baes, C. F.; Mesmer, R. E. *The hydrolysis of cations*; Wiley Interscience: New York, 1976.
(24) Plummer, L. N.; Busenberg, E. *Geochim. Cosmochim. Acta* **1982**, *46*, 1011−1040.
(25) Gómez-Morales, J.; Torrent-Burgués, J.; López-Macipe, A.; Rodriguez-Clemente, R. *J. Cryst. Growth* **1996**, *166*, 1020−1026.
(26) Ruiz-Agudo, E.; Putnis, C. V.; Rodriguez-Navarro, C.; Putnis, A. *Geochim. Cosmochim. Acta* **2011**, *75*, 284−296.
(27) Hong, M.; Teng, H. H. *Geochim. Cosmochim. Acta* **2014**, *141*, 228−239.
(28) Stack, A. G.; Grantham, M. C. *Cryst. Growth Des.* **2010**, *10*, 1409−1413.
(29) Perdikouri, C.; Putnis, C. V.; Kasioptas, A.; Putnis, A. *Cryst. Growth Des.* **2009**, *9*, 4344−4350.
(30) Wolf, S. E.; Müller, L.; Barrea, R.; Kampf, C. J.; Leiterer, J.; Panne, U.; Hoffmann, T.; Emmerling, F.; Tremel, W. *Nanoscale* **2011**, *3*, 1158−116.

DOI: 10.1021/acs.cgd.6b00276
Cryst. Growth Des. 2016, 16, 4173−4177